

## CHAPTER 134

### LOCAL SCOUR AROUND A LARGE CIRCULAR CYLINDER DUE TO WAVE ACTION

Eiichi Saito

Research Engineer, Tech. Res. Inst., Hazama-Gumi Ltd.

Shinji Sato and Tomoya Shibayama

Associate Professor, Yokohama National University  
156 Tokiwadai, Hodogaya-ku, Yokohama 240, JAPAN

#### 1. Introduction

In the construction of large-scale maritime structures, the prediction of scouring around the foundation is essential to examine the stability of the structures. The local scour around a large circular cylinder is closely related to problems encountered in the construction of offshore artificial island and large-scale piers and is thus very important from engineering point of view.

The mechanism of local scours at the base of breakwaters as well as small circular cylinders has been investigated mainly by laboratory experiments [*e.g.* Irie and Nadaoka(1984), Bijker and Bruyn (1988)]. The mechanism of sand movement around a large circular cylinder was also investigated experimentally by Katsui and Toue(1988). However, there seems to be no model to predict bottom profile change around large-scale structures, the dimension of which is comparable to the wavelength, since the wave field around them is complicated owing to the presence of diffracted waves.

The aim of the present study is to propose a numerical model to estimate the topographical change around a large circular cylinder installed in the wave field. The validity of the model will be confirmed with laboratory experiments.

#### 2. Experimental Procedures

Experiments were performed in a 9 x 9 m wave basin as shown in Fig. 1. A 2 x 2 m test section enclosed with a wooden frame was installed in the basin. Well-sorted sand of 0.2 mm in median diameter was filled in the test bed on which a circular cylinder of 52.2 cm in diameter was installed. The water depth at the test bed was 16.5cm. A continuous-type bottom profiler and capacitance-type

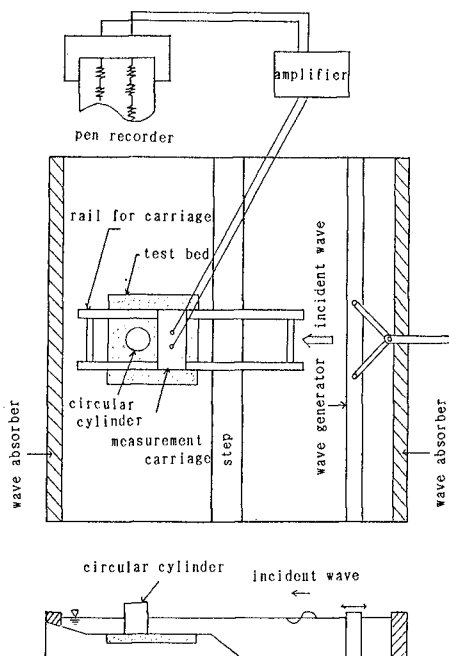


Fig. 1 Experimental Equipment

wave gages were installed on a measurement carriage as shown in Fig. 1. The wave and current field as well as bottom profile change were measured in detail for two monochromatic wave conditions listed in Table 1, where  $H$  represents incident wave height and  $T$  the wave period.

#### (1) Distribution of Wave Height

The distribution of wave height was measured systematically at grid points situated with a horizontal spacing of 10 cm. The measurements were carried out from 0 to 1 hour and from 4 to 6 hours upon the initiation of wave action.

#### (2) Test Bed Topography

The bottom profile in the test bed was measured by using a bottom profiler installed on the measurement carriage. The carriage was allowed to move in

Table 1 Experimental Conditions

case	1	2
$T$ (sec)	0.94	0.94
$H$ (cm)	6.7	7.9
$h$ (cm)	16.5	16.5

parallel to the wave incidence so that the bottom profile along the measuring line was measured. The measuring line interval was set to be 5 cm near the circular cylinder and 10 cm for the other areas. The measurements were carried out at 1, 2, 4 and 6 hours after wave generation. The scouring depth along the cylinder surface was also measured.

### (3) Current

The direction and the magnitude of the current developed around the cylinder were measured by tracing the movement of dye particles.

### (4) Sand Movement Mechanism

The sand in front of the cylinder was replaced with sand colored with white paint so that the sand movement and suspension were easily observed.

## 3. Numerical Model

A numerical model was developed for the bottom topography change around a large circular cylinder. The model consisted of three submodels, that is, wave model, current model and sand transport model. In the present study, the model was developed on the assumption that the change of sand surface level was small compared with the initial water depth so that the wave and current field were not changed drastically even after bottom deformation. The present model is therefore applicable only to the sand movement in early stages, where the change in the topography around the circular cylinder was small compared to the water depth.

### (1) Wave model

The wave field was evaluated by using the linear diffraction theory presented by McCamy Fuchs(1954). The velocity potential  $\phi$  expressed in the cylindrical coordinate defined in Fig. 2 was given by

$$\phi = -\frac{igH}{2\omega} \frac{\cosh k(h+z)}{\cosh kh} \left[ \sum_m \varepsilon_m i^m \left\{ J_m(kr) - \frac{J'_m(kr_0)}{H_m^{(1)'}(kr_0)} H_m^{(1)}(kr) \right\} \cos m\theta \right] \quad (1)$$

where  $\omega$  denotes the angular frequency,  $k$  the wave number,  $h$  the water depth,  $r_0$  the diameter of the cylinder and  $J_m(kr)$  and  $H_m^{(1)}(kr)$  are the Bessel and the Hankel function of the first kind respectively. The symbol  $i$  represents the imaginary number unit and  $\varepsilon_m$  is unity for  $m = 0$  and 2 for otherwise. Near-bottom velocity and the radiation stress were evaluated analytically by using the theoretical wave field.

### (2) Current model

The net movement of sand is influenced by the two current velocities, that is, the depth-integrated current induced by the spatial variation of the radiation stress and the mass transport velocity in the vicinity of the bed. The mass transport velocity  $\vec{U}_m = (U_{mr}, U_{m\theta})$  at the edge of the bottom boundary layer was evaluated by the following equation which was converted from the laminar

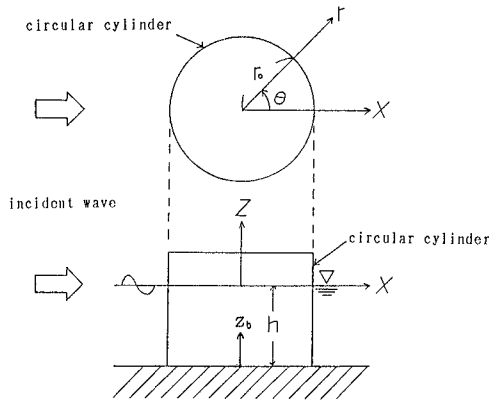


Fig. 2 Definition of Coordinates

solution for compound waves in the Cartesian coordinate presented by Carter et al. (1973) to the cylindrical coordinate  $(r, \theta)$ :

$$U_{mr} = -\frac{1}{4\omega} [F_5 u_r \frac{\partial u_r^*}{\partial r} + F_6 u_\theta \frac{1}{r} (\frac{\partial u_r}{\partial \theta} - u_\theta)^* + F_7 \frac{u_r}{r} (\frac{\partial u_\theta}{\partial \theta} + u_r)^*] \quad (2)$$

$$U_{m\theta} = -\frac{1}{4\omega} [F_5 \frac{u_\theta}{r} (\frac{\partial u_\theta}{\partial \theta} + u_r)^* + F_6 u_r \frac{\partial u_\theta^*}{\partial r} + F_7 u_\theta \frac{\partial u_r^*}{\partial r}] \quad (3)$$

where  $u_r$  and  $u_\theta$  represents the amplitude of the radial and the tangential components of the orbital velocity and the symbol \* denotes complex conjugate. The symbols  $F_5$ ,  $F_6$  and  $F_7$  are complex constants such that  $F_5 = -3 + 5i$ ,  $F_6 = -1 + 2i$  and  $F_7 = -2 + 3i$ .

A compound wave field with a complex wave height distribution was observed around the large circular cylinder. The spatial variation of the radiation stress therefore seemed to induce a stationary current field around the cylinder. This stationary current velocity  $\vec{U} = (U_r, U_\theta)$  was determined through numerical calculation using depth integrated conservation equation of mass and momentum, expressed by the cylindrical coordinates as follows:

$$\frac{\partial \bar{\zeta}}{\partial t} + \frac{1}{r} \frac{\partial}{\partial r} [r U_r (h + \bar{\zeta})] + \frac{1}{r} \frac{\partial}{\partial \theta} [U_\theta (h + \bar{\zeta})] = 0 \quad (4)$$

$$\frac{\partial U_r}{\partial t} + U_r \frac{\partial U_r}{\partial r} + \frac{U_\theta}{r} \frac{\partial U_r}{\partial \theta} + F_r - M_r + R_r + g \frac{\partial \bar{\zeta}}{\partial r} = 0 \quad (5)$$

$$\frac{\partial U_\theta}{\partial t} + U_r \frac{\partial U_\theta}{\partial r} + \frac{U_\theta}{r} \frac{\partial U_\theta}{\partial \theta} + F_\theta - M_\theta + R_\theta + \frac{g}{r} \frac{\partial \bar{\zeta}}{\partial \theta} = 0 \quad (6)$$

where  $\bar{\zeta}$  denotes the mean water level and  $t$  the time. The symbols  $F_r$  and  $F_\theta$

denote the friction term given by the following equation respectively:

$$F_r = \frac{f}{\rho(h + \zeta)} U_r \quad (7)$$

$$F_\theta = \frac{f}{\rho(h + \zeta)} U_\theta \quad (8)$$

where  $f$  is the friction coefficient expressed by

$$f = \frac{2}{\pi} \rho C_f u_b \quad (9)$$

where  $C_f$  denotes the bottom friction coefficient,  $u_b$  the orbital velocity amplitude near the bottom and  $\rho$  the density of fluid.

Terms  $M_r$  and  $M_\theta$  represent lateral diffusion expressed by

$$M_r = \frac{1}{r} \frac{\partial}{\partial r} (\varepsilon r \frac{\partial U_r}{\partial r}) + \frac{1}{r^2} (\varepsilon \frac{\partial^2 U_r}{\partial \theta^2}) \quad (10)$$

$$M_\theta = \frac{1}{r} \frac{\partial}{\partial r} (\varepsilon r \frac{\partial U_\theta}{\partial r}) + \frac{1}{r^2} (\varepsilon \frac{\partial^2 U_\theta}{\partial \theta^2}) \quad (11)$$

where  $\varepsilon$  denotes the diffusion coefficient. The value of  $\varepsilon$  was assumed to be  $100 \text{ cm}^2/\text{s}$  in the present study.

The symbols  $R_r$  and  $R_\theta$  represent the gradient of radiation stress expressed by

$$R_r = \frac{1}{\rho(h + \zeta)} \left( \frac{\partial S_{rr}}{\partial r} + \frac{1}{r} \frac{\partial S_{r\theta}}{\partial \theta} \right) \quad (12)$$

$$R_\theta = \frac{1}{\rho(h + \zeta)} \left( \frac{\partial S_{\theta r}}{\partial r} + \frac{1}{r} \frac{\partial S_{\theta\theta}}{\partial \theta} \right) \quad (13)$$

where  $S_{rr}$ ,  $S_{\theta\theta}$ ,  $S_{r\theta}$  and  $S_{\theta r}$  represent components of the radiation stress tensor.

### (3) Sand transport model

The sand transport rate was modeled in terms of the bottom shear stress and near-bottom current velocity. The Shields parameter  $\psi_m$  was expressed by

$$\psi_m = \frac{1}{2} \frac{f_w u_b^2}{s g d} \quad (14)$$

where  $f_w$  denotes the friction coefficient proposed by Jonsson (1966),  $s$  ( $=1.65$ ) the specific gravity of sand in water and  $d$  the diameter of sand particle. Water particles near the bottom move in general in elliptic orbits under compound wave field and there are many unknown factors involved in the estimation of the friction factor. The friction factor was estimated in the present study by using maximum wave orbital velocity.

Using the mass transport velocity  $\vec{U}_m$ , stationary current velocity  $\vec{U}$  and the Shields parameter  $\psi_m$ , the volumetric net sand transport rate  $\vec{q}$  per unit width was assumed to be estimated by the following equation:

$$\vec{q} = A(\psi_m - \psi_c)(\vec{U}_m + \alpha\vec{U})d \frac{1}{1 - \lambda_v} \quad (15)$$

where  $\psi_c$  represents the critical Shields parameter for the general movement of sand particles,  $\lambda_v$  the void ratio of sediment and the symbols  $A$  and  $\alpha$  denote non-dimensional coefficients. The coefficient  $\alpha$  is a parameter which represents the ratio of the contribution to  $\vec{q}$  of  $\vec{U}$  to that of  $\vec{U}_m$ . The mass transport velocity  $\vec{U}_m$  represents the steady drift velocity at the edge of the bottom boundary layer while the stationary current velocity  $\vec{U}$  is depth-integrated velocity calculated assuming that the velocity is uniform over entire water depth. In reality, the current profile is not uniform and therefore the velocity near the bottom is considered to be smaller than that of the averaged velocity. It is thus considered that the influence on the sand movement by the mass transport is greater than that of the stationary current and therefore the value of  $\alpha$  is expected to be smaller than unity.

The net sand transport rate was considered to be also affected by local sea bed gradient. The net sand transport rate  $\vec{Q}$  was expressed by the following equation by introducing the influence of the sea bed gradient in the same way as proposed by Watanabe et al.(1986):

$$\vec{Q} = \vec{q} - \epsilon_s |\vec{q}| \nabla z_b \quad (16)$$

where  $z_b$  denotes the bed level and  $\epsilon_s$ , a non-dimensional coefficient.

The change of bottom topography was calculated by using the mass conservation equation of the sediment.

$$\frac{\partial z_b}{\partial t} = -\nabla \vec{Q} \quad (17)$$

The numerical calculation was carried out by using a finite difference method with a calculation grid as shown in Fig. 3. Every derivative in the governing equations was replaced with a central difference in the computation.

## 4. Results

### (1) Wave Field

Figure 4 shows the distribution of relative wave height which was the ratio of local wave height to the incident wave height. Figure 4 (a) was measured from 0 to 1 hour after the initiation of wave action and Fig. 4(b) from 4 to 6 hours. The wave field by the linear diffraction theory is shown in Fig. 4(c). No great difference is noticed in Fig.4 (a) and Fig.4 (b), which means that no great

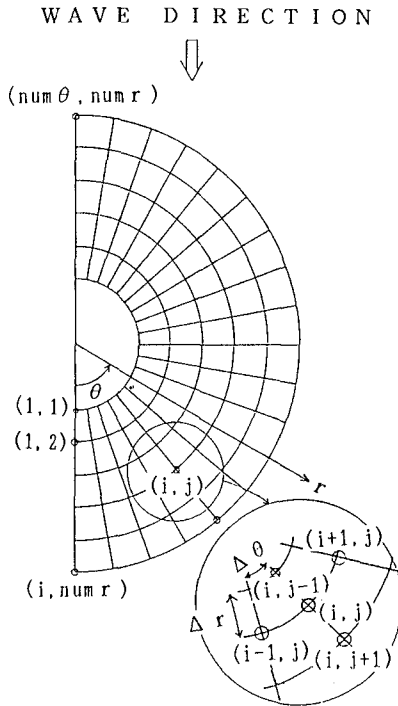


Fig. 3 Calculation Grid

variation in the wave field was developed even when the bed topography varies with time. This implies that the assumption made in the numerical models was almost completely satisfied for the condition of present experiments. The overall agreement between the measurement and the theory supports the validity of the wave model.

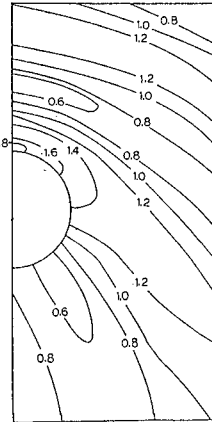
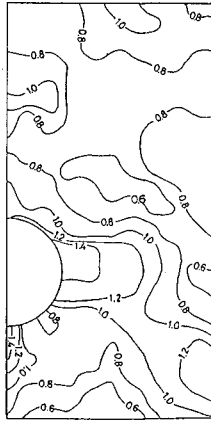
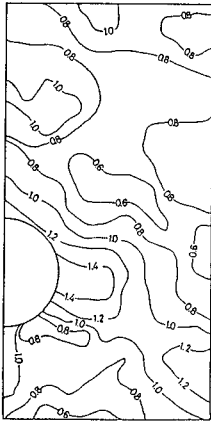
## (2) Current Field

Since the current field around the circular cylinder was very complicated, it was very difficult to quantitatively measure the current velocity by tracing injected dye. However, it was observed that there existed a stationary current field as shown in Fig. 5(a). In Fig. 5(a), the large arrow represents the current direction and the arrow given by the continuous line represents the displacement of water particles near the bottom due to wave orbital motion. Figure 5(b) shows the computation of the mass transport velocity and Fig. 5(c) gives the computation of the stationary current velocity. According to these figures, the calculated stationary current velocities agree well with the observed velocity field.

WAVE DIRECTION



CASE 1	
H	= 6.7
T	= 0.94
h	= 16.5



(a) Measured ( from 0 to 1 hour after wave action ) (b) Measured ( from 4 to 6 hours after wave action ) (c) Calculation

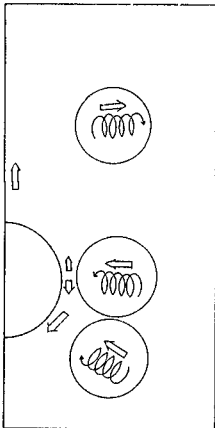
Fig. 4 Distribution of Wave Height

WAVE DIRECTION

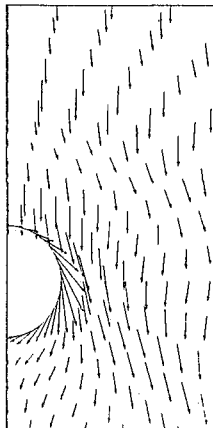


H	= 7.9 (m)
T	= 0.94 (s)
h	= 16.5 (cm)

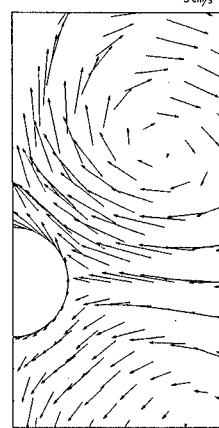
5 cm/s



(a) Measured



(b) Distribution of computed mass transport velocity



(c) Distribution of computed stationary current

Fig. 5 Distribution of Current ( Case 2, Waves are incident from the top. )

## (3) Test Section Topography

Figure 6 shows a comparison of the calculated bottom topography with the measurement. The hatched areas in the figure indicate the scoured area. Since it took approximately 4 hours for bottom topography to reach equilibrium for the condition shown in this figure, the numerical computation were carried out for 4 hours. The coefficient  $A$  was set at 0.07,  $\epsilon_s$  at 0.03 and the critical Shields parameter  $\psi_c$  at 0.06. Figure 6 (a) shows the measurement, Fig. 6(b) the calculation assuming that  $\alpha$  be unity and Fig. 6(c) the calculation when  $\alpha$  is 0.2.

Since the influence of the stationary current is overestimated in Fig. 6(b), the calculation shows a considerably different topographical variation. Compared Fig. 6(b) and (c) with Fig. 6(a), we can conclude that the numerical model can predict the local scour pattern when  $\alpha$  was fixed at 0.2. However, some discrepancies are noticed especially in the area just in front of the circular cylinder. The reasons for the discrepancy will be discussed in the below.

Firstly, there seems to be a problem in the estimation of the Shields parameter. The wave field around the circular cylinder is so complicated that water particles near the bottom move in two-dimensional orbits shaped circle, ellipse and straight line. Therefore, there seems to be inadequacy in estimating the Shields parameter  $\psi_m$  and critical Shields parameter  $\psi_c$  in an analogy to one dimensional oscillatory flow.

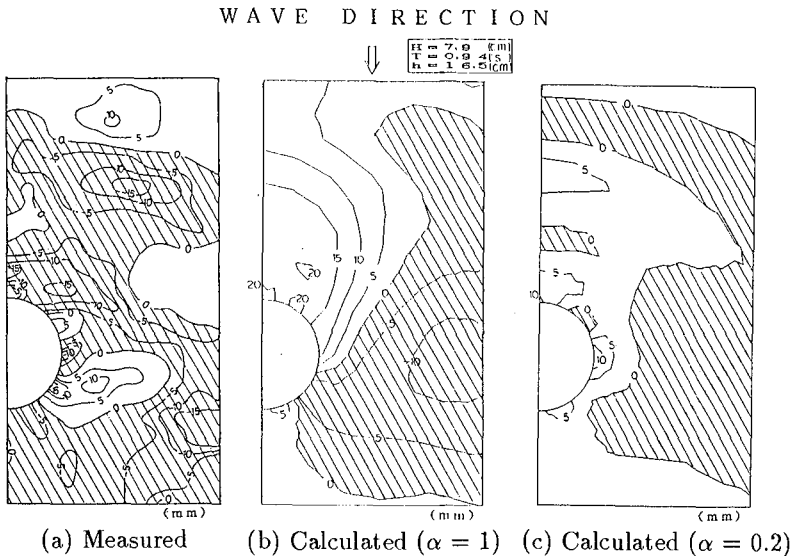


Fig. 6 Bottom Topographies ( Case 2, 4 hours after wave action)

Second reason for the discrepancy is due to the use of the linear wave theory. The effect of wave asymmetry was not involved in the model since the near-bottom velocity was estimated by using the linear theory. Remarkable discrepancy is noticed just in front of the cylinder where standing waves were formed. According to Irie and Nadaoka(1984), which investigated the sea bed deformation in front of a breakwater, the direction of sand movement under standing waves was determined by the mass transport velocity and the asymmetry in near-bottom velocity variation. Waves observed in the experiments were relatively high so that the nonlinearity of wave is another factor which should be involved in the model.

### 5. Concluding remarks

Laboratory experiments were performed in a wave basin to reproduce the local sea bed scour around large-scale maritime structures. Experiments suggested that the mass transport velocity and wave-induced steady currents were essential in modeling sand transport. Based on experimental observations, a numerical model was presented for the local scour around a large circular cylinder. The applicability of the model was confirmed with experiments. Although some discrepancies are still present between experiments and computation, the model seems to provide a basic framework for the local scour around large-scale structures. Future studies are expected on the three-dimensional boundary layer flow as well as on the wave nonlinearity.

### 6. References

- Bijker, E. W. and C. A. de Bruyn (1988): Erosion around a pile due to current and breaking waves, Proc. 21st ICCE, pp. 1368-1381.
- Carter, T. G., P. L. F. Liu and C. C. Mei(1973): Mass transport by waves and offshore sand bedforms, J. WW, ASCE, No.99, pp. 165-184.
- Irie, I. and K. Nadaoka (1984): Laboratory reproduction of seabed scour in front of breakwaters, Proc. 19th ICCE, pp. 1715-1731.
- Jonsson, I. G. (1966): Wave boundary layers and friction factors, Proc. 10th ICCE, pp. 127-148.
- Katsui, H. and T. Toue (1988): Inception of sand motion around a large obstacle, Proc. 21st ICCE, pp. 1280-1294.
- McCamy, R. C. and R. A. Fuchs (1954): Wave forces on piles, B.E.B. Tech. Memo., No. 69.
- Watanabe, A., K. Maruyama, T. Shimizu and T. Sakakiyama (1986): Numerical prediction model of three-dimensional beach deformation around a structure, Coastal Eng. in Japan, Vol. 29, pp. 179-194.